Check for updates

Received: 5 June 2024 | Revised: 5 July 2024 | Accepted: 8 July 2024

DOI: 10.1002/ardp.202400455

FULL PAPER

ARCH PHARM DPhG
Archiv der Pharmazie

Natural flavonoids as promising lactate dehydrogenase A inhibitors: Comprehensive in vitro and in silico analysis

Ümit Yırtıcı

Department of Medical Laboratory, Kirikkale University, Kirikkale, Turkey

Correspondence
Ümit Yırtıcı, Vocational School of Health Services, Department of Medical Laboratory, Kirikkale University, TR-71450 Kirikkale, Turkey.
Email: umityirtici@kku.edu.tr

Funding information
None

Abstract

The inhibitory potential of 17 flavonoids on lactate dehydrogenase A (LDHA), a key enzyme in the downstream process of aerobic glycolysis in cancer cells, is investigated. Fisetin exhibited excellent inhibitory activity (IC_{50} = 0.066 μM). Quercetin 3-β-D-glucoside, quercetin 3-galactoside, luteolin, neoeriocitrin, and luteolin 7-*O*-β-D-glucoside showed good inhibitory activity (IC_{50} = 1.397–15.730 μM). Biochanin A, baicalein, quercetin, scutellarein-7-glucuronide, diosmetin, baicalein 7-*O*-β-D-glucuronide, and apigenin 7-apioglucoside demonstrated moderate inhibitory activity (IC_{50} = 33.007–86.643 μM). Eriodictyol, quercetin 7-*O*-β-D-glucoside, apigenin 7-*O*-β-D-glucoside, and epicatechin were inactive. The Lineweaver–Burk plot showed that fisetin competitively inhibits NADH binding (K_i = 0.024 μM). K_i values for other compounds were calculated using the Cheng–Prusoff equation (K_i = 0.2799–2.1661 μM). The study revealed that the inhibitory effect of flavonoids varies with the number and position of OH groups and bound sugars. Molecular docking analyses indicated that flavonoids exhibited strong interactions with the NADH binding site of LDHA through hydrophobic interactions and hydrogen bonds. Molecular dynamic simulations tested the stability of the fisetin-LDHA complex over 100 ns and showed fisetin's high binding affinity to LDHA, maintaining strong hydrogen bonds. The binding energy of fisetin with LDHA was −33.928 kcal/mol, indicating its effectiveness as an LDHA inhibitor. Consequently, flavonoids identified as strong inhibitors could be potential cancer treatment sources through LDHA inhibition.

KEYWORDS
enzyme inhibition, flavonoids, lactate dehydrogenase A, molecular docking, molecular dynamics

1 | INTRODUCTION

Cancer is a disease that involves various processes, including cell proliferation, invasion, resistance to cell death, angiogenesis, and evasion from the immune system. Despite the availability of many treatments, resistance to conventional therapies, such as chemotherapy and radiotherapy, remains a significant challenge in cancer treatment. One of the factors contributing to this resistance is the metabolic reorganization that occurs in cancer cells, leading to an affair known as the "Warburg effect," or aerobic glycolysis. Aerobic

This is an open access article under the terms of the Creative Commons Attribution License, which permits use, distribution and reproduction in any medium, provided the original work is properly cited.
© 2024 The Author(s). *Archiv der Pharmazie* published by Wiley-VCH GmbH on behalf of Deutsche Pharmazeutische Gesellschaft.

glycolysis promotes lactate production, even in oxygen, and is regulated primarily by lactate dehydrogenase (LDH). LDH5 (LDHA) is an isoform of LDH that plays a critical role in the metabolic switch in cancer cells. It catalyzes the reduction of pyruvate to lactate and maintains a glycolytic pathway by oxidizing NADH to NAD^+. Restoring NAD^+ in cancer cells promotes lactate secretion into the microenvironment, decreasing extracellular pH and inducing invasion, immunosuppression, angiogenesis, and metastasis, leading to a poor prognosis in cancer. Inhibition of LDHA is a promising strategy for reducing tumor growth and overcoming chemoresistance. Recent studies have focused on developing highly potent and selective LDHA inhibitors for cancer therapy.[1–4]

Flavonoids are secondary metabolites derived from plants that benefit human health. These effects include antioxidant, antiangiogenic, and anticancer properties.[5] Additionally, several studies demonstrate that flavonoids are natural inhibitors of LDH. For example, galloflavin, a flavanol analog, reduces the proliferation of human colon cancer SW620 cells and various breast cancer cells by occupying the NADH binding site of LDHA. Green tea's (–)-epigallocatechin gallate inhibits LDHA in MIA PaCa-2 pancreatic cancer cells, disrupting the cellular metabolic network and conferring anticancer activity.

Similarly, (–)-epigallocatechin, a precursor to (–)-epigallocatechin gallate, significantly inhibits breast cancer growth and induces apoptosis by acting as an LDHA inhibitor. Morin successfully reduces cancer initiation and proliferation in MCF-7 and MDA-MB-231 cells by inhibiting the enzymatic function of LDH. Luteolin 7-*O*-β-D-glucoside is found to block a type of human LDH and has the potential for use in cancer therapy. Various flavonoids, such as quercetin, luteolin, tectoridin, iristectorin A, iridin, tectorigenin, irigenin, irisfluorentin, acetyldaidzin, malonylgenistin, daidzin, glycitin, genistin, acetylglycitin, daidzein, and tectorigenin-7-*O*-β-D xylosylglucoside, also show potential for decrease LDHA levels in different cancer cell types.[6,7] Therefore, flavonoids are potential candidates for inhibiting LDHA, and research into the inhibitory properties of more flavonoids for LDHA appears to be a strategic target in cancer treatment.

This study investigated the potential in vitro inhibition properties of 17 different types of flavonoids for LDHA. In silico studies were performed to determine the interactions and binding properties of the flavonoids with the enzyme.

TABLE 1 IC_{50} and K_i values of flavonoids against lactate dehydrogenase A (LDHA).

Number	Flavonoid	IC_{50} (μM)	Cheng–Prusoff equation K_i (μM)
1	Fisetin	0.066 ± 0.00^a	0.0017 ± 0.00^a
2	Quercetin 3-β-D-glucoside	1.397 ± 0.10^b	0.0349 ± 0.01^b
3	Quercetin 3-glalactoside	1.447 ± 0.12^b	0.0362 ± 0.01^b
4	Luteolin	1.792 ± 0.15^b	$0{,}0448 \pm 0.01^b$
5	Neoeriocitrin	11.198 ± 0.90^c	$0{,}2799 \pm 0.04^c$
6	Luteolin 7-*O*-glucoside	15.730 ± 1.20^d	$0{,}3934 \pm 0.05^d$
7	Biochanin a	33.007 ± 2.33^e	0.8252 ± 0.08^e
8	Baicalein	33.485 ± 2.41^e	0.8371 ± 0.08^e
9	Quercetin	33.647 ± 2.52^e	0.8412 ± 0.09^e
10	Scutellarein-7-glucuronide	38.508 ± 2.60^{ef}	0.9627 ± 0.10^e
11	Diosmetin	42.009 ± 2.89^f	1.0502 ± 0.12^{ef}
12	Baicalein 7-*O*-glucuronide	59.754 ± 2.98^g	1.4939 ± 0.29^f
13	Apigenin 7-apioglucoside	86.643 ± 3.45^h	2.1661 ± 0.48^g
14	Eriodictyol	231.049 ± 5.46^i	Na
15	Quercetin 7-glucoside	Na	Na
16	Apigenin 7-*O*-glucoside	Na	Na
17	Epicatechin	Na	Na

Note: Different lowercase letters in the same column indicate significant differences in IC_{50} and K_i values ($p < 0.05$). na, not active.

2 | RESULTS AND DISCUSSION

2.1 | Enzyme inhibition

The potential of some flavonoid groups to inhibit the LDHA enzyme was investigated, and the results are presented in Table 1 and Figure 1. Based on the IC_{50} values, the compounds were classified into five categories: excellent potential (<1 μM), good potential (1–20 μM), moderate potential (20–100 μM), low activity (100–200 μM), and inactive (>200 μM). Accordingly, fisetin was an excellent inhibitor (IC_{50} = 0.066 μM), while quercetin 3-β-D-glucoside (IC_{50} = 1.397 μM), quercetin 3-galactoside (IC_{50} = 1.447 μM), luteolin (IC_{50} = 1.792 μM), neoeriocitrin (IC_{50} = 11.198 μM), and luteolin 7-*O*-β-D-glucoside (IC_{50} = 15.730 μM) demonstrated good inhibitory potential (Figure 1a,c). Biochanin A, baicalein, quercetin, scutellarein-7-glucuronide, diosmetin, baicalein 7-*O*-β-D-glucuronide, and apigenin 7-apioglucoside exhibited moderate potential, with IC_{50} values between 33.007 and 86.643 μM (Figure 1d). Eriodictyol (IC_{50} = 231.049 μM), quercetin 7-*O*-β-D-glucoside, apigenin 7-*O*-β-D-glucoside, and epicatechin were found to be inactive.

The experimentally obtained data were utilized to ascertain the nature of the enzyme inhibition by fisetin via Lineweaver–Burk plots and to calculate the K_i constants (inhibitory constants). As illustrated in Figure 1b, fisetin competitively inhibits NADH binding to the enzyme LDHA with K_i values of 0.024 ± 0.0001 μM. This value is consistent with the K_i value obtained by the Cheng-Prusoff equation (K_i = 0.0017 ± 0.0022 μM). This result indicates that the molecule affects the substrate binding site.

The K_i values for other compounds were calculated using the Cheng-Prusoff equation for the NADH binding site. The K_i values for

15214184, 2024, 9, Downloaded from https://onlinelibrary.wiley.com/doi/10.1002/ardp.202400455 by Kirikkale University, Wiley Online Library on [30/06/2025]. See the Terms and Conditions (https://onlinelibrary.wiley.com/terms-and-conditions) on Wiley Online Library for rules of use; OA articles are governed by the applicable Creative Commons License

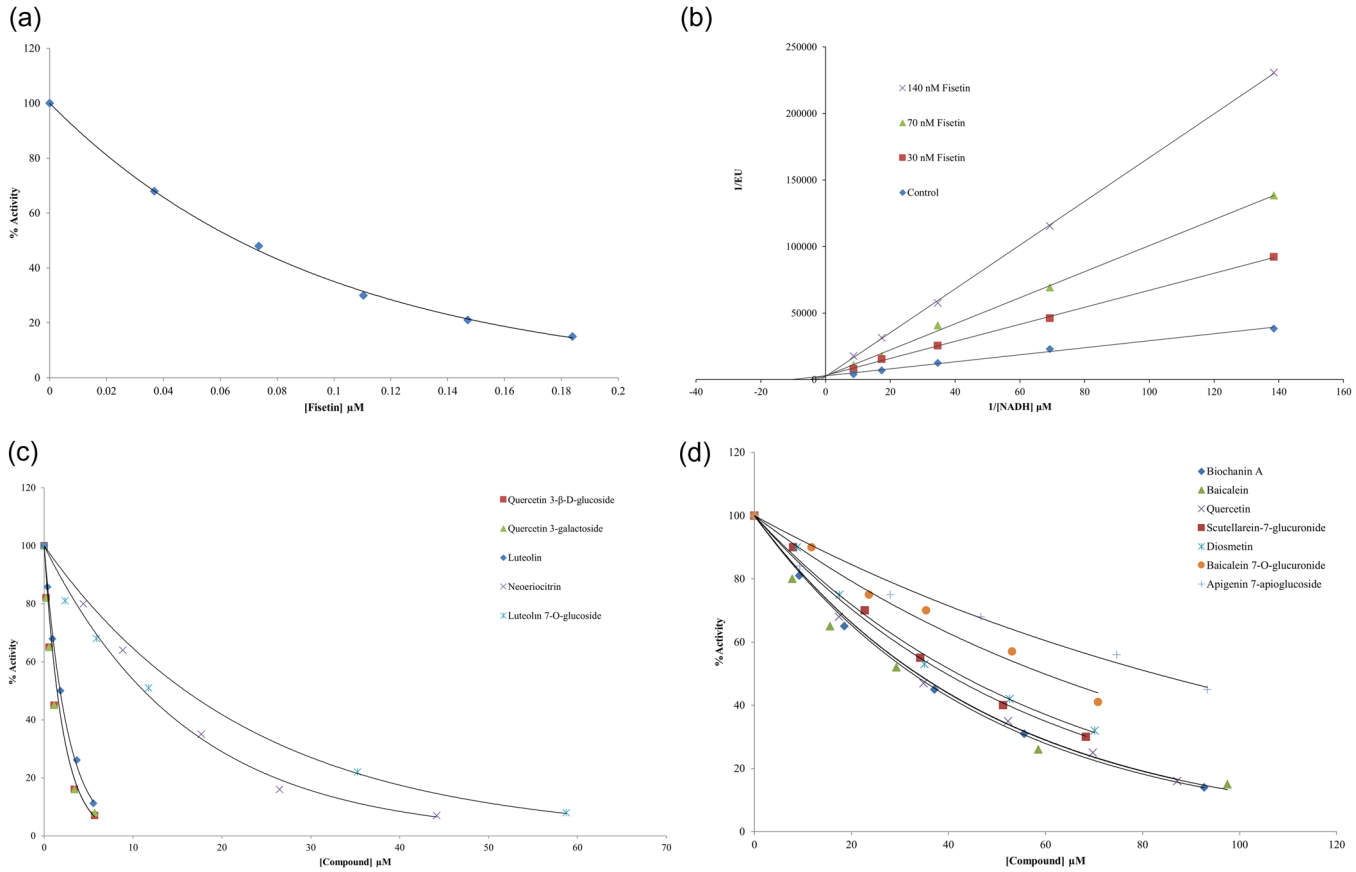

FIGURE 1 The results of in vitro studies. (a) Inhibition plot of fisetin, (b) Lineweaver-Burk plot of fisetin, (c) Inhibition plots of quercetin 3-quercetin 3-β-D-glucoside, quercetin 3-galactoside, luteolin, neoeriocitrin and luteolin 7-O-β-D-glucoside, (d) Inhibition plots of biochanin A, baicalein, quercetin, scutellarein-7-glucuronide, diosmetin, baicalein 7-O-β-D-glucuronide, and apigenin 7-apioglucoside.

quercetin 3-β-D-glucoside, quercetin 3-galactoside, and luteolin were found to be 0.0349 and 0.0448 µM, respectively. The K_i values of flavonoids other than eriodictyol, quercetin 7-*O*-D-glucoside, apigenin 7-*O*-β-D glucoside, and epicatechin ranged between 0.2799 and 2.1661 µM. For the indicated target, compounds with K_i values < 1 µM can be considered potential inhibitors, while molecules with K_i values between 1 and 10 µM can be precursor compounds to synthesize more active molecules. According to these values, these compounds can be considered LDHA inhibitors or new lead compounds to design specific potential inhibitors.[5,8]

Previous studies have demonstrated that certain flavonoids can inhibit LDHA at the cellular level, reducing LDHA production in cancer cells.[3,9] However, there are only a limited number of studies in which the inhibition properties of flavonoids on LDHA and IC_{50} and K_i values have been determined experimentally. One such study is that of galloflavin, a reference molecule.[10] The IC_{100} value of galloflavin for LDHA was 201 µM, while a K_i value of 56 µM was obtained against NADH. In studies of other flavonoids, the IC_{50} value for luteolin 7-*O*-β-D-glucoside was 139.2 µM, while the K_i value against NADH was 68 µM. The IC_{50} value for morin was 7.2 µM, and the K_i value against pyruvate was also found to be 7.2 µM.[11,12] In this study, the IC_{50} value for luteolin 7-*O*-β-D-glucoside was 15.730 µM, while the K_i value against NADH was 0.3934 µM. Fisetin is demonstrated to regulate glucose homeostasis by reducing LDH activity in diabetic rats and positively affecting glucose metabolism and insulin secretion.[13] Furthermore, fisetin is effective against numerous cancer cell lines and pathways that may lead to cancer.[14] This study also revealed that fisetin has potent LDHA inhibitory properties, with IC_{50} and *K*i values being first determined.

The inhibitory capacity of the flavonoids included in the study varied according to the structure and position of the substituents attached to the flavonoid rings. The fact that glucose and galactose sugars (quercetin 3-β-D-glucoside; IC_{50} = 1.397 µM, K_i = 0.0349 µM, quercetin 3-*O*-galactoside; IC_{50} = 1.447 µM, K_i = 0.0362 µM) increased the inhibitory effect of these molecules, but the inhibitory effect of this compound (quercetin 7-*O*-β-D-glucoside), which has the same flavone skeleton but the binding of glucose sugar to the C-7 position of the A ring, decreased the inhibitory effect. In our study, while the IC_{50} value of baicalein molecule was found to be 33.485 µM (K_i = 0.8252 µM), the binding of the sugar group containing ester group to the C-7 position of baicalein 7-*O*-β-D-glucuronide compound increased the IC_{50} value approximately twofold to 59.754 µM (K_i = 1.4939 µM). In this case, the binding of the ester group-containing sugar molecule to the baicalein molecule at the C-7 position decreased the inhibition value. Again, the IC_{50} value of luteolin (K_i = 0.0448 µM) was 1.792 µM, while the IC_{50} value of the derivative, luteolin 7-*O*-β-D-glucoside (K_i = 0.3934), of the

15214184, 2024, 9, Downloaded from https://onlinelibrary.wiley.com/doi/10.1002/ardp.202400455 by Kirikkale University, Wiley Online Library on [30/06/2025]. See the Terms and Conditions (https://onlinelibrary.wiley.com/terms-and-conditions) on Wiley Online Library for rules of use; OA articles are governed by the applicable Creative Commons License

same compound containing a glycoside group at the C-7 position increased to 15.730 µM. So this means that the inhibition effect decreased approximately tenfold. Therefore, monosaccharides bound at different positions to the flavonoids studied caused significant differences in enzyme inhibition. In addition to the different functional groups contained in the glucose or galactose compounds in the flavonoid compound, it has been shown that the different positioning of these glucose or galactose groups causes the compounds to reach favorable conformations to enter the active site of the enzyme due to the steric effect on the molecule, which leads to a change in the inhibition effects after settling in the active site.[15–17] The A and C rings of flavonoids with OH functional groups are essential in inhibiting the enzyme. Comparative analysis of fisetin, luteolin, and quercetin revealed that, unlike quercetin, the presence of a single hydroxyl group on the A ring of fisetin and the C ring of luteolin was effective in enhancing the enzyme inhibition effects of these compounds.

2.2 | Molecular docking

The crystal structure of LDHA was downloaded from the Protein Data Bank (PDB code: 5W8L) and used to predict the possible molecular interaction between the compounds and the enzymes. NADH was found to interact with the active catalytic site. It was repositioned to the active site of the crystal; the best-scoring docked pose was used as a starting point for molecular docking studies. Flavonoids were placed in the active site of LDHA with equal parameters and gaps where NADH and LDHA bind. The docking details of flavonoids and NADH with the best conformations are listed in Tables 2 and 3. Moldock scores were also given in Table 4.

Flavonoids, due to their OH groups and monosaccharide groups attached to their third position, appear to interact strongly with amino acid residues in the docking site of the adenine base and adenine-ribose sugar of NADH and bind with higher affinity. The interaction details of fisetin, luteolin, quercetin 3-β-D-glucoside, and quercetin 3-galactoside, which have a high inhibitory effect against the LDHA enzyme in the experimental results, are given in Figures 2 and 3. In addition, the interaction details of NADH are also given together with these compounds in Figures 2 and 3.

It is seen that fisetin and luteolin, quercetin 3-β-D-glucoside and quercetin 3-galactoside show similar localization properties. Fisetin bound to the catalytic site with a MolDock score of −107.842 in Molegro Virtual Docker. Fisetin exhibited H-bonds with residues GLY96, THR94, GLY28 × 2, and GLY26 of LDHA via B and C rings. It also showed electrostatic interaction with ASP51 × 2 residue through B and C rings. However, numerous hydrophobic interactions were predicted with residues ALA95 × 3, VAL52 × 2, ILE119, and ILE115 through rings A, B, and C. Van der Waals interactions were also found with residues ARG98, ILE53, ALA97, PHE118, TYR82, and VAL50. Similar to fisetin, luteolin showed more hydrophobic interactions (ALA95 × 3, VAL52 × 2, ILE115, ILE119) and formed fewer hydrogen bonds (GLY28 × 2, THR94, ILE115, GLY96). Like fisetin, it showed electrostatic interactions with the ASP51 × 2 residue. The fact that fisetin and luteolin are located close to the region where the adenine base of NADH is located and show similar numerous hydrophobic interactions with amino acids seems to be the main reason for their inhibition effects. However, it is noteworthy that the second OH group attached to the A ring of luteolin does not interact. It seems to be the reason for the lower inhibitory effect of luteolin compared to fisetin in the experimental results.

Quercetin 3-β-D-glucoside formed hydrogen bridges with residues GLY31 × 2, GLY96 × 2, THR94 × 2, GLY28 × 2, GLY245, VAL135, ARG98, ASN137, mainly through the OH group of the monosaccharide attached to the third position. However, it showed fewer hydrophobic interactions over residues VAL30 × 2, ALA29, ILE251, and TYR246. A similar situation was predicted for quercetin 3-galactoside. It formed a large number of hydrogen bonds with residues GLY96 × 3, THR94 × 3, GLY28 × 2, ARG98 × 2, ALA95, ALA29, GLY245, ASN137, SER136, mainly through the OH group of the monosaccharide at third position in its structure. At the same time, it showed fewer hydrophobic interactions (TYR246) and electrostatic interactions (ARG98×2). The monosaccharide parts of quercetin 3-β-D-glucoside and quercetin 3-galactoside show more hydrogen bonding interactions with regions of NADH other than the adenine base through similar amino acids, which may account for their more significant inhibition effects compared to quercetin.

In contrast, as Figure 4 illustrates, luteolin 7-*O*-β-D-glucoside, the monosaccharide derivative of luteolin linked to the seventh position, and quercetin 7-*O*-β-D-glucoside, the monosaccharide derivative of quercetin linked to the seventh position, exhibited reduced interaction with the amino acid residues. A comparable situation is observed in baicalein and its derivative, baicalein 7-*O*-β-D-glucuronide, which contains a monosaccharide linked to the seventh carbon. The discrepancy in the inhibitory effects between these compounds can be attributed to the differences in their positioning at the active center, which is influenced by steric effects and the distinct types and numbers of bonds formed.

2.3 | Molecular dynamic simulations of LDHA protein, as apoprotein and in complex with 5W8L-fisetin

To assess the binding interactions of 5W8L-fisetin, a series of molecular dynamics (MD) simulations were carried out. Each simulation ran for 100 ns and included two models: the apoprotein LDHA and the 5W8L-fisetin complex, as depicted in Figure 5. From the molecular structure and topographic analysis of the apoprotein and protein–ligand complex, as depicted in Figure 5a, it can be seen that the fisetin molecule is well-compatible with the 5W8L protein. Furthermore, the 2D interaction analysis of the first frame of MD revealed that the residual interaction around the fisetin was strong and rigid with H-bonds and other interactions (Figure 5b,c). The simulations enabled a comprehensive analysis encompassing a range of statistical parameters, including root-mean-square deviation (RMSD), root-mean-square fluctuation (RMSF), and the characterization of hydrogen bond interactions and their occupancy percentages throughout the simulations.

15214184, 2024, 9, Downloaded from https://onlinelibrary.wiley.com/doi/10.1002/ardp.202400455 by Kirikkale University, Wiley Online Library on [30/06/2025]. See the Terms and Conditions (https://onlinelibrary.wiley.com/terms-and-conditions) on Wiley Online Library for rules of use; OA articles are governed by the applicable Creative Commons License

TABLE 2 The interaction details of fisetin, quercetin 3-β-D-glucoside, quercetin-3-galactoside, and luteolin with lactate dehydrogenase A (LDHA) active cavity.

		Fisetin		Quercetin 3-β-D-glucoside		Quercetin-3-galactoside		Luteolin	
Types	Category	Residues	Distance	Residues	Distance	Residues	Distance	Residues	Distance
Hydrogen bond	Conventional hydrogen bond	GLY96	1.79	GLY31	1.67	ALA29	1.78	THR94	2.01
		THR94	2.07	GLY96	1.81	GLY96	1.81	GLY28	2.18
				GLY245	2.13	GLY245	1.87		
				THR94	2.15	THR94	1.93		
				THR94	2.19	THR94	2.18		
				VAL135	2.21	GLY96	2.25		
				GLY28	2.36	ASN137	2.29		
				ARG98	2.38	GLY28	2.30		
				GLY28	2.57	ARG98	2.39		
				ASN137	2.71				
	Carbon hydrogen bond	GLY28	2.27	THR94	1.92	THR94	1.84	ILE115	2.65
		GLY26	2.63	GLY31	2.98	GLY28	2.60	GLY28	2.92
		GLY28	2.79	GLY96	3.02	ALA95	2.67		
						SER136	2.70		
						GLY96	2.75		
						ARG98	3.08		
	Pi-Donor hydrogen bond							GLY96	3.05
Electrostatic	Pi-Anion	ASP51	3.59					ASP51	3.36
		ASP51	4.26					ASP51	4.31
	Pi-Cation					ARG98	4.06		
						ARG98	4.84		
Hydrophobic	Pi-Alkyl	ALA95	3.32	VAL30	4.23			ALA95	3.50
		VAL52	4.14	VAL30	4.41			VAL52	4.03
		ALA95	4.23	ALA29	5.21			VAL52	4.17
		VAL52	4.40	ILE251	5.45			ALA95	4.45
		ILE119	4.71					ILE115	4.58
		ILE115	5.08					ILE119	4.76
		ALA95	5.14					ALA95	4.86
		VAL25	5.45						
	Pi-Pi Stacked			TYR246	4.87	TYR246	5.02		

2.3.1 | RMSD analysis

The RMSD provides significant insights into the structural alterations experienced by the protein and the ligand throughout the simulation period. Figure 6 illustrates the RMSD of the protein across time for two separate simulations. The complex molecule rapidly attained a stable phase rather than an apoprotein of 5W8L, as evidenced by RMSD values falling below 0.5 nm, and it was all stable throughout the simulation.

RMSD values of the ligand in the apoprotein form provide valuable insights into the stability of their interactions with the protein. Figure 7 depicts a multiplot graph of the RMSD of the ligands throughout all simulations. Notably, the ligand consistently exhibits RMSD values below 0.4 nm, remaining almost stable around 0.2 nm. In contrast, the RMSD stability of the apoprotein form was variable, with RMSD values exceeding 0.4 nm. Therefore, the fisetin-5W8L complex displayed RMSD values within acceptable limits, indicating its effective binding ability with the LDHA protein.

15214184, 2024, 9, Downloaded from https://onlinelibrary.wiley.com/doi/10.1002/ardp.202400455 by Kirikkale University, Wiley Online Library on [30/06/2025]. See the Terms and Conditions (https://onlinelibrary.wiley.com/terms-and-conditions) on Wiley Online Library for rules of use; OA articles are governed by the applicable Creative Commons License

TABLE 3 The interaction details of NADH sites with lactate dehydrogenase A (LDHA).

NADH					
Site		**Types**	**Category**	**Residues**	**Distance**
Adenine ribonucleotide	Adenine	Hydrogen bond	Conventional hydrogen bond	VAL52	3.06
			Carbon hydrogen bond	GLY96	3.43
		Hydrophobic	Pi-Alkyl	VAL52	3.87
				ALA95	3.90
				ALA95	4.00
				VAL52	4.22
				ILE115	4.51
				ILE115	5.24
				ILE119	5.27
	Ribose	Hydrogen bond	Conventional hydrogen bond	GLY96	2.26
				ASP51	2.64
				ASP51	2.69
			Carbon hydrogen bond	ALA95	2.28
				ASP51	3.27
	Phosphate	Hydrogen bond	Conventional hydrogen bond	ARG98	2.02
			Carbon hydrogen bond	GLY28	2.65
				GLY96	3.63
		Hydrogen bond: electrostatic	Salt bridge: attractive charge	ARG98	2.18
Nicotinamide nucleotide	Nicotinamide	Hydrogen bond	Conventional hydrogen bond	VAL135	3.00
			Carbon hydrogen bond	VAL135	3.06
			Pi-Donor hydrogen bond	HIS192	3.61
		Electrostatic	Pi-Cation	HIS192	4.32
		Hydrophobic	Pi-Alkyl	ILE251	4.27
				VAL30	4.85
	Ribose	Hydrogen bond	Conventional hydrogen bond	ASN137	1.87
				ASN137	2.12
			Carbon hydrogen bond	SER136	2.68
	Phosphate	Hydrogen bond	Conventional hydrogen bond	VAL30	2.01
				ALA29	2.93
			Carbon hydrogen bond	GLY28	2.40
				THR94	3.20

2.3.2 | RMSF analysis

RMSF provides valuable insights into localized structural changes. Figure 8 presents a multiplot graph illustrating the protein's RMSF, measured in nanometers, corresponding to the residue number index. Notably, this graph indicates less than 0.6 nm fluctuations for most protein residues, affirming the overall structural stability. Upon comparison of the fluctuation values between the apoprotein and fisetin-5W8L complex, it became evident that higher fluctuations were observed, particularly in the protein region PRO128-ILE134, ARG164-HIS185, and MET203-GLU235 throughout the 100 ns simulation period. It indicates that intermolecular interactions are elevated in these residue regions, conferring more excellent stability to the complex structure than in the apoprotein form.

15214184, 2024, 9, Downloaded from https://onlinelibrary.wiley.com/doi/10.1002/ardp.202400455 by Kirikkale University, Wiley Online Library on [30/06/2025]. See the Terms and Conditions (https://onlinelibrary.wiley.com/terms-and-conditions) on Wiley Online Library for rules of use; OA articles are governed by the applicable Creative Commons License

TABLE 4 MolDock scores of active compounds.

Number	Compound	Ligand	MolDock score
1	Fisetin	5,281,614	−107.842
2	Quercetin 3-β-D-glucoside	44,259,136	−114.136
3	Quercetin 3-galactoside	5,281,643	−113.143
4	Luteolin	5,280,445	
5	Neoeriocitrin	1,14,627	−131.792
6	Luteolin 7-O-glikozit	5,280,637	−138.781
7	Biochanin a	5,280,373	−101.776
8	Baicalein	5,281,605	−103.368
9	Quercetin	5,280,343	−106.406
10	Scutellarein 7-glucuronide	185,617	−114.427
11	Diosmetin	5,281,612	−111.493
12	Baicalein 7-O-glucuronide	64,982	−117.882
13	Apigenin 7-apioglucoside	5,280,746	−148.528

2.3.3 | H-bond interaction

The comprehension of molecular interactions, particularly hydrogen bonds (H-bonds), is contingent upon the parameters of distance and angle and is susceptible to the influence of dynamic conditions. This investigation analyzed the H-bond interactions within the 5W8L apoprotein and 5W8L-fisetin complex. Figure 9 illustrates a plot demonstrating the number of hydrogen bonds over time. It is evident from the plot that fisetin exhibited more robust and consistent H-bond interactions throughout the simulation than the apoprotein. The percentage of occupancies of specific residues engaged in these hydrogen bond interactions was calculated to gain further insight into these interactions and assess their stability.

Figure 10 presents a histogram of the percentage occupancies of H-bond contacts formed by different ligands. This graph illustrates the fisetin-5W8L complex's ability to establish multiple interactions with PRO165, ASP178, TYR163, and ILE215, with occupancy rates of 81.35%, 89.42%, 88.32%, and 77.05%, respectively. A comparison of the occupancy rates with LDHA residues reveals that fisetin forms a more effective and stable complex structure with the protein, with

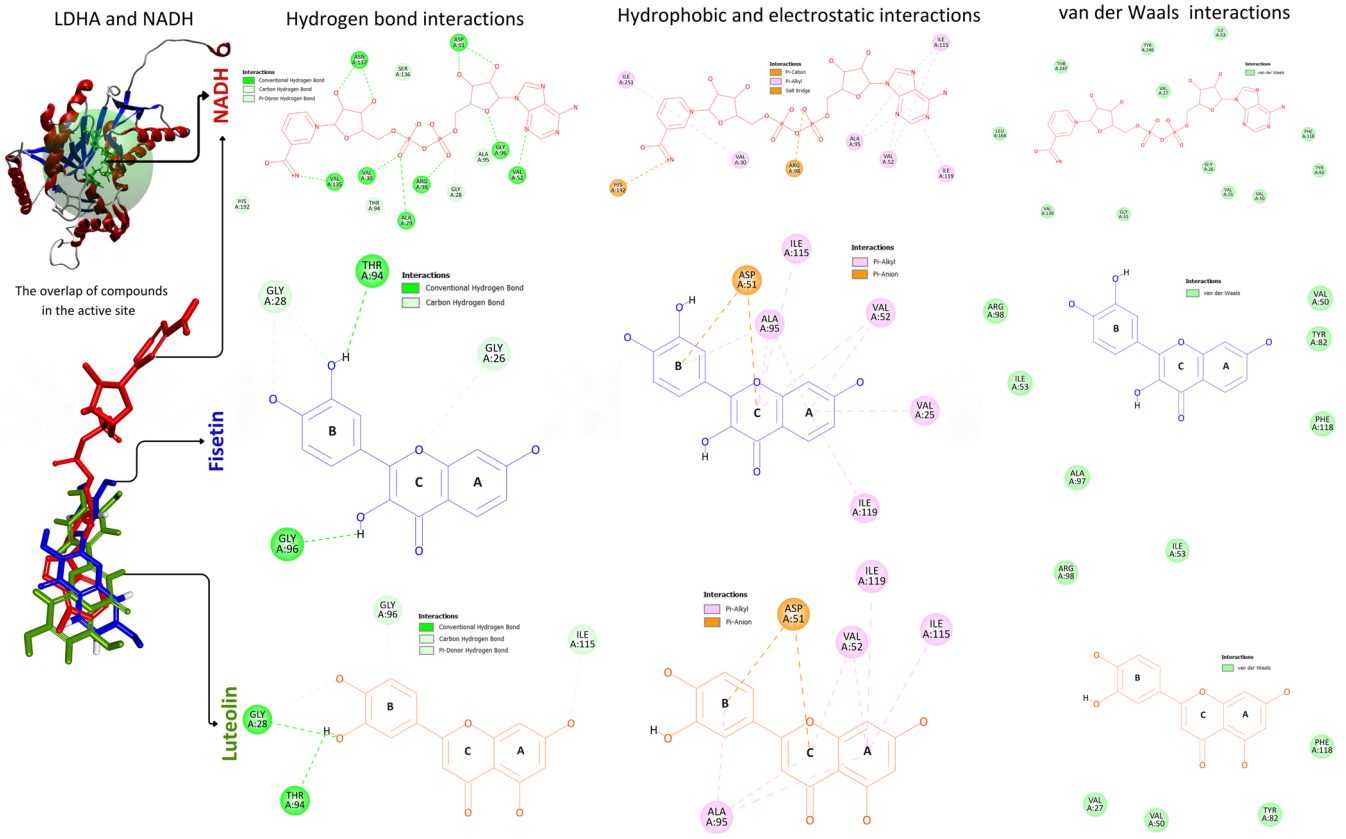

FIGURE 2 Three-dimensional (3D) and two-dimensional (2D) interaction maps of NADH, fisetin, and luteolin with the lactate dehydrogenase A (LDHA) active cavity.

15214184, 2024, 9, Downloaded from https://onlinelibrary.wiley.com/doi/10.1002/ardp.202400455 by Kirikkale University, Wiley Online Library on [30/06/2025]. See the Terms and Conditions (https://onlinelibrary.wiley.com/terms-and-conditions) on Wiley Online Library for rules of use; OA articles are governed by the applicable Creative Commons License

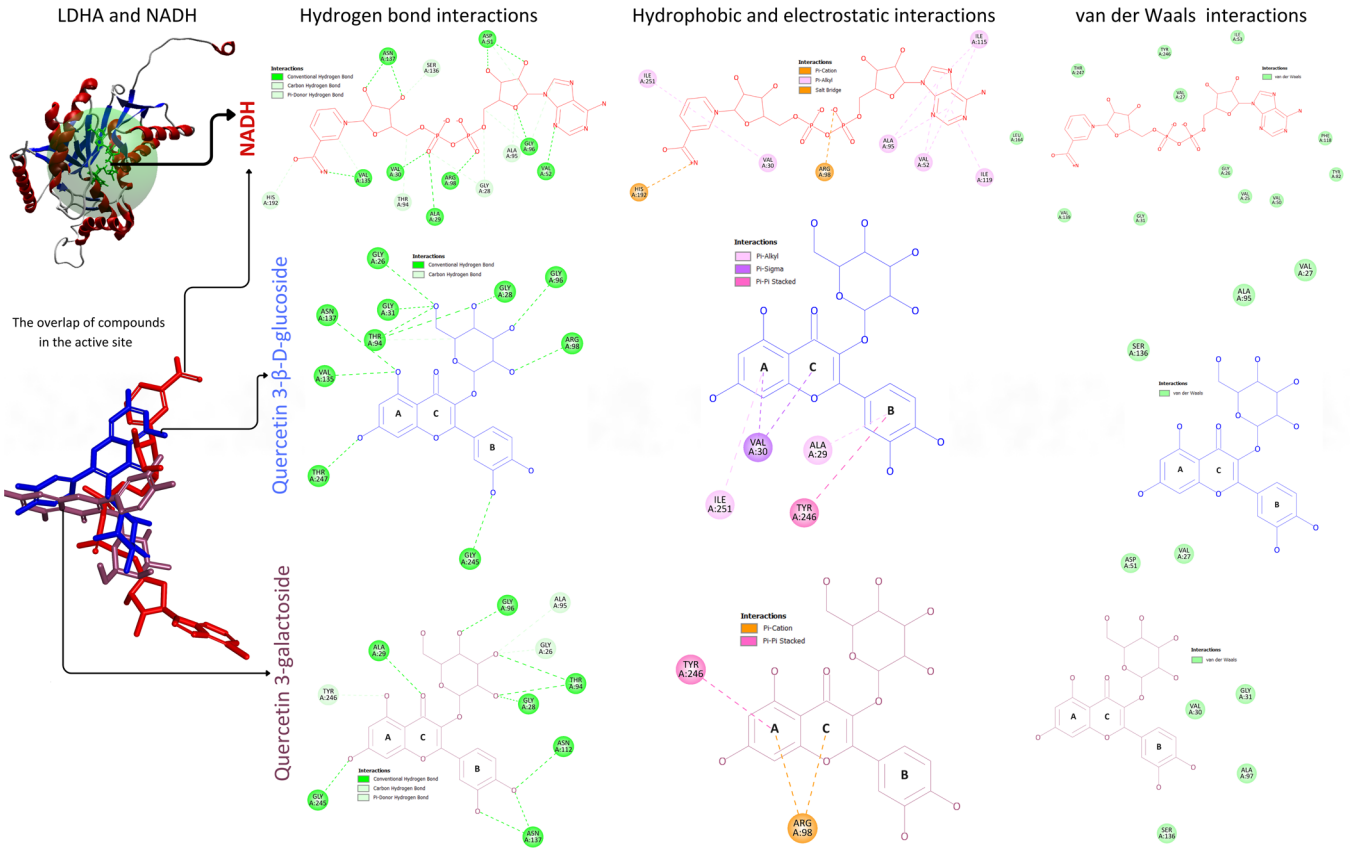

FIGURE 3 Three-dimensional (3D) and two-dimensional (2D) interaction maps of NADH, quercetin 3-β-D-glucoside, and quercetin 3-galactoside with the lactate dehydrogenase A (LDHA) active cavity.

higher occupancy rates towards the residues. These findings suggest that fisetin binds most efficiently with the LDHA protein.

2.3.4 | MMGBSA calculations

As part of the molecular dynamics investigation, a thorough energetics analysis is important in explaining the protein–ligand complex stability. Therefore, an molecular mechanics-generalized born surface area (MMGBSA) calculation was performed on the simulation cluster. This analysis revealed average ΔG0 values of apoprotein 5W8L and fisetin-5W8L complex as −27.236 and −33.928 kcal/mol, respectively (Table 5 and Figure 11). These results indicate that fisetin is more efficient than other compounds in binding with the LDHA protein. With such findings, fisetin emerges as a promising candidate for future pharmacological studies, particularly for its potential as an anticancer agent.

3 | CONCLUSION

This study highlights the potential of flavonoids as inhibitors of LDHA, a critical enzyme in cancer cell metabolism. The investigation revealed that flavonoids, particularly fisetin, quercetin 3-β-D-glucoside, quercetin 3-galactoside, and luteolin, exhibit significant inhibitory effects on LDHA. Fisetin emerged as the most potent inhibitor, demonstrating an IC_{50} of 0.066 µM and a competitive inhibition constant (K_i) of 0.024 µM, indicating its capability to effectively compete with NADH at the binding site. Additionally, the study revealed essential data indicating that the inhibition effects of flavonoids may vary according to their OH groups and the position of sugars attached to flavonoids. Molecular docking and dynamics simulations provided further insights into the interactions between these flavonoids and LDHA, highlighting the stability and strong binding affinities of the complexes formed, especially for fisetin. The findings from MMGBSA calculations supported the superior binding efficiency of fisetin, reinforcing its potential as a leading candidate for LDHA inhibition. The study suggests that targeting LDHA with flavonoid-based inhibitors could be a promising strategy to overcome and inhibit tumor growth. These findings call for further pharmacological investigations to explore the therapeutic applications of flavonoids in cancer treatment, with the potential for developing novel anticancer agents.

4 | MATERIALS AND METHODS

The chemicals utilized in this study were procured from Sigma-Aldrich Company.

15214184, 2024, 9, Downloaded from https://onlinelibrary.wiley.com/doi/10.1002/ardp.202400455 by Kirikkale University, Wiley Online Library on [30/06/2025]. See the Terms and Conditions (https://onlinelibrary.wiley.com/terms-and-conditions) on Wiley Online Library for rules of use; OA articles are governed by the applicable Creative Commons License

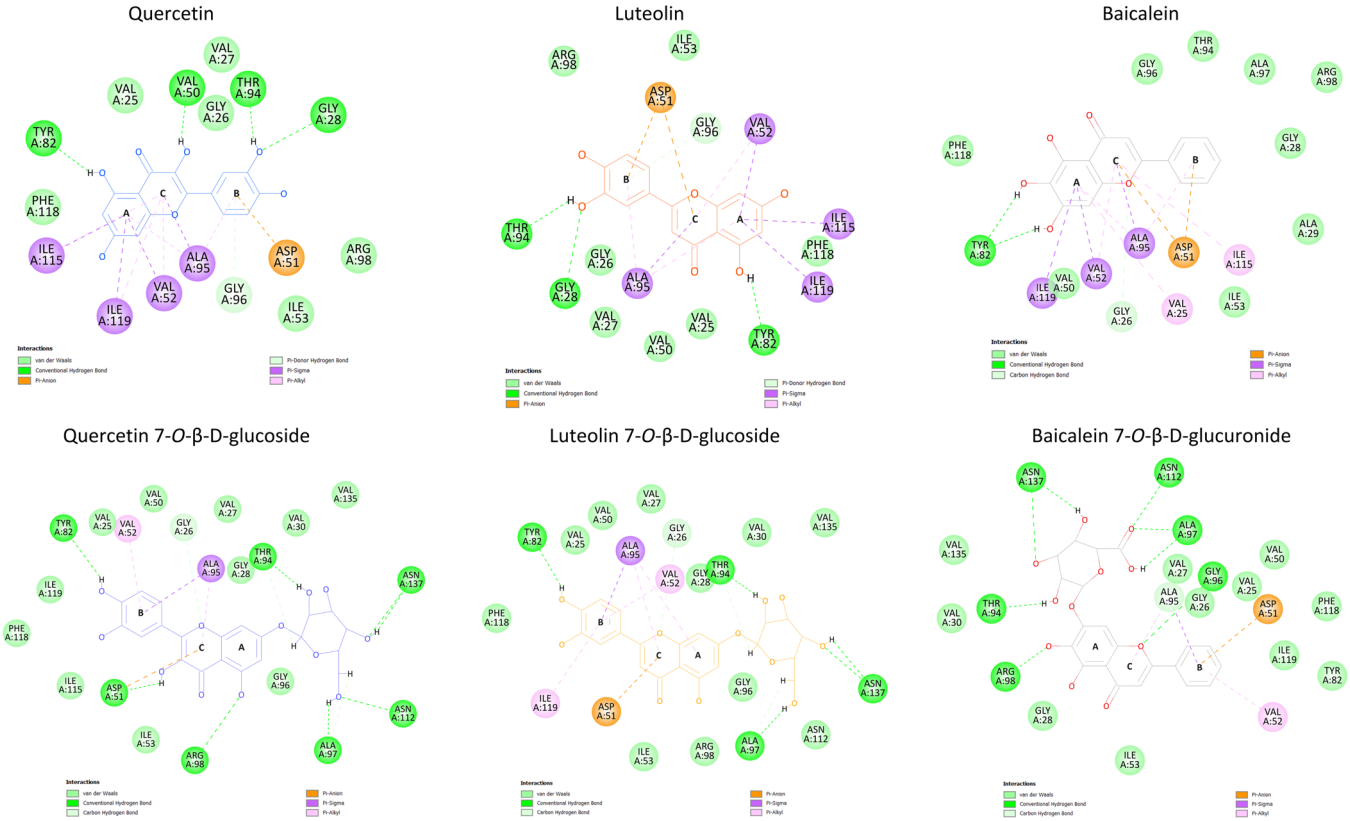

FIGURE 4 Two-dimensional (2D) interaction maps of quercetin, luteolin, baicalein, quercetin 7-*O*-β-D-glucoside, luteolin 7-*O*-β-D-glucoside, and baicalein 7-*O*-β-D-glucuronide with the lactate dehydrogenase A (LDHA) active cavity.

4.1 | Enzyme inhibition assay

The inhibitory potential of flavonoids against LDHA was monitored via in vitro kinetic assays. The activity of LDHA was quantified by measuring the conversion of NAD+ to NADH via the microplate reader with a wavelength of 340 nm.[18] Pyruvic acid served as the substrate. A total of 50 µL of buffer (Tris-HCl 0.6 M, pH 7.3), 40 µL of 3 mM NADH, 50 µL of different concentrations of flavonoids, and 10 µL of enzyme solution were transferred to a well of a plate. Subsequently, the reaction was incubated at 25°C for 15 min, after which 20 µL of 6 mM Pyruvic acid was added. The absorbance change of the wells was recorded at 37°C for 10 min—the enzyme activity in the absence of an inhibitor served as the control. The enzyme activity was tested in the presence of increasing concentrations of compounds, and the resulting %activity-[concentration] graphs were plotted using the values obtained using the Microsoft Excel program, according to the absorbance values obtained. IC_{50} values were calculated from the graph curves. The inhibition type and K_i constants of fisetin against LDHA were determined by measuring its activity with five different NADH concentrations in the 6–240 nM range using saturated substrate concentration at three different inhibitor concentrations. Lineweaver Burk plots were used to calculate the inhibition type and *Ki* constants. K_i values for other compounds were calculated using the Cheng–Prusoff equation.[19]

4.2 | Molecular docking

The Molegro Virtual Docker software was employed to ascertain the potential interactions between flavonoids and LDHA.[20] The X-ray structure was obtained from the Protein Data Bank (PDB) with the ID 5W8L (https://www.rcsb.org/structure/5W8L).[21] Before docking, the protein structure was edited using the software's protein preparation tool. The coordinates utilized for docking were −14.41, 25.25, and −36.7 for binding sites *x*, *y*, and *z*, respectively. The radius for the NADH binding site was 14 Å. The docking procedure was validated by repositioning the X-ray ligand to the active site with the docking program. The three-dimensional structures of flavonoids were downloaded in SDF format from the web platform https://pubchem.ncbi.nlm.nih.gov. Docking experiments were performed 10 times for each molecule, and the binding model with the highest predicted score was selected to examine the molecular interaction details. Visualization of the optimal docking results was performed using Discovery Studio 2021 Client.

4.3 | Molecular dynamic (MD) simulation

MD simulation was carried out using GROMACS 2022.2. The following steps were utilized.

15214184, 2024, 9, Downloaded from https://onlinelibrary.wiley.com/doi/10.1002/ardp.202400455 by Kirikkale University, Wiley Online Library on [30/06/2025]. See the Terms and Conditions (https://onlinelibrary.wiley.com/terms-and-conditions) on Wiley Online Library for rules of use; OA articles are governed by the applicable Creative Commons License

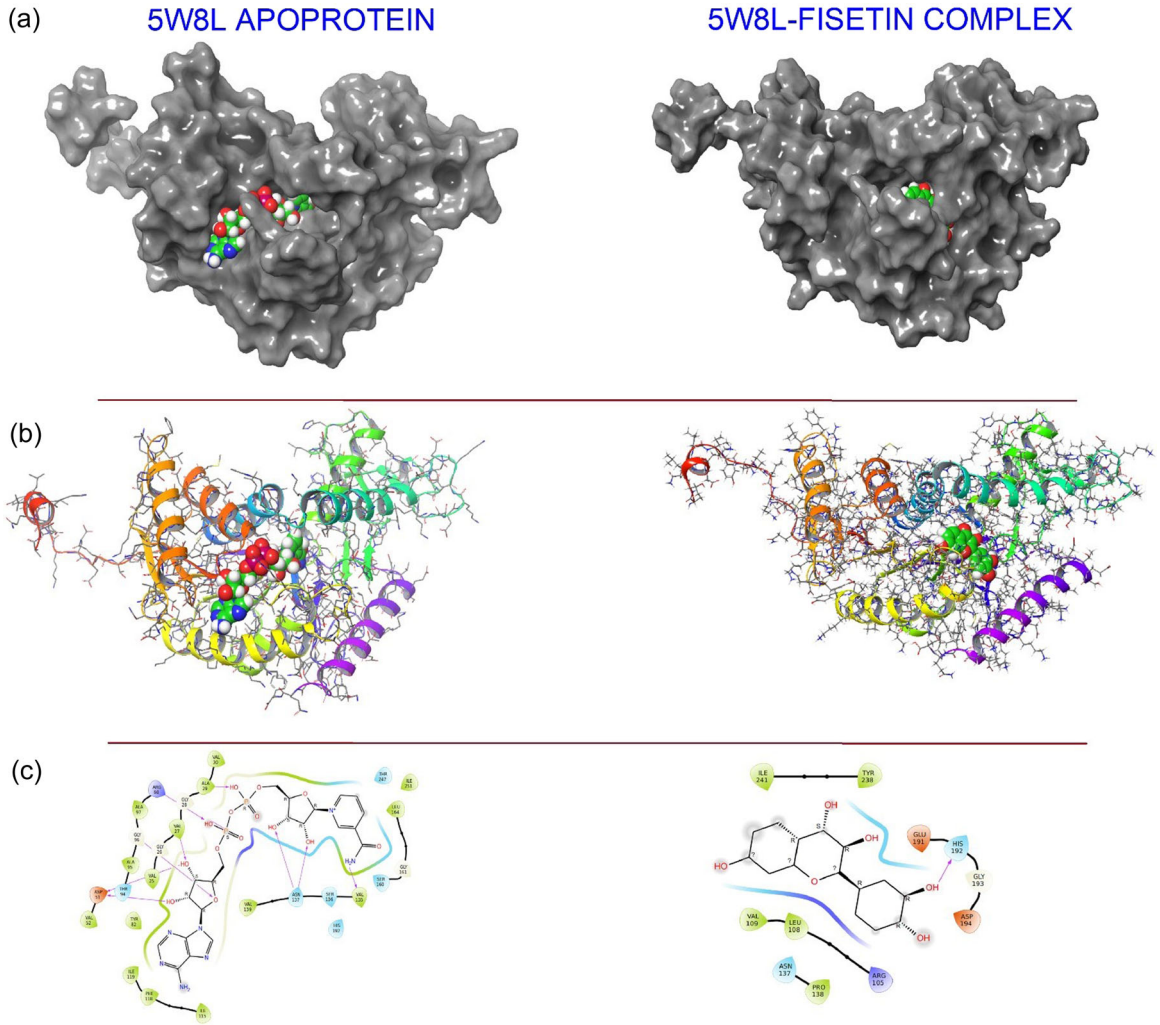

FIGURE 5 Graphical representation of protein-ligand complexes for 5W8L apoprotein and fisetin-5W8L complex: (a) Surfacial representation of protein and protein-ligand complex, (b) Molecular and secondary structural representation of protein and protein-ligand complex, (c) 2D interaction diagram of protein and protein–ligand complex.

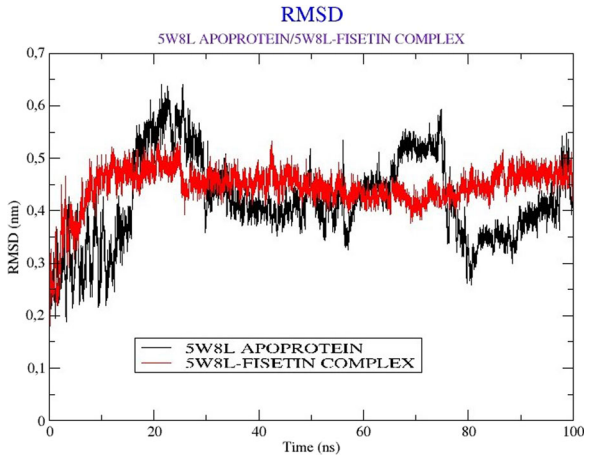

FIGURE 6 Graphical representation of the plots showing protein root-mean-square deviation (RMSD) (nm) versus time (100 ns) for 5W8L apoprotein and fisetin-5W8L complex.

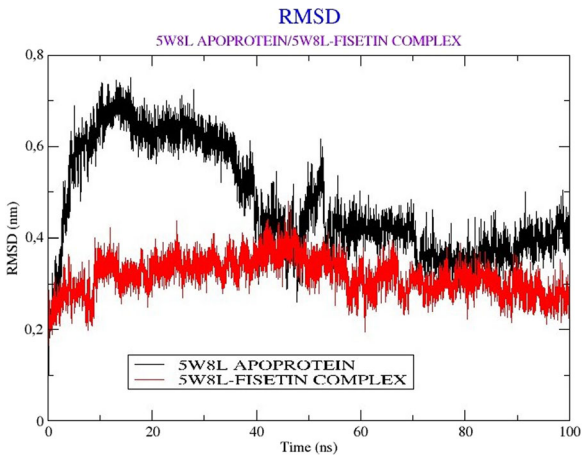

FIGURE 7 Graphical representation of the plots showing Ligand root-mean-square deviation (RMSD) (nm) versus time (100 ns) for 5W8L apoprotein and fisetin-5W8L complex.

15214184, 2024, 9, Downloaded from https://onlinelibrary.wiley.com/doi/10.1002/ardp.202400455 by Kirikkale University, Wiley Online Library on [30/06/2025]. See the Terms and Conditions (https://onlinelibrary.wiley.com/terms-and-conditions) on Wiley Online Library for rules of use; OA articles are governed by the applicable Creative Commons License

4.3.1 | Preparation of enzyme

The 3-dimensional (3D) models of apoprotein and ligand-protein complexes were exported to.pdb format using Pymol. The dynamic behavior of the complexes was evaluated using MD simulation in the GROMACS package program (version 2022.2).[22–24] Protein topology was constructed by pdb2gmx with the CHARMM27 force field,[25] and ligand topology was generated using the SwissParam server.[26]

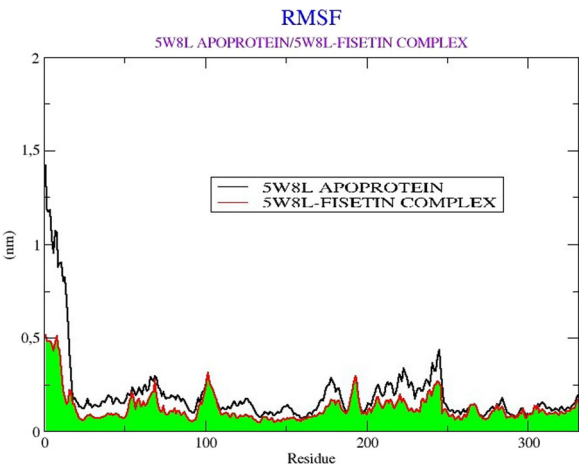

FIGURE 8 Graphical representation of the plots showing the protein RMSF (nm) versus residue index number of protein for 5W8L apoprotein and fisetin-5W8L complex.

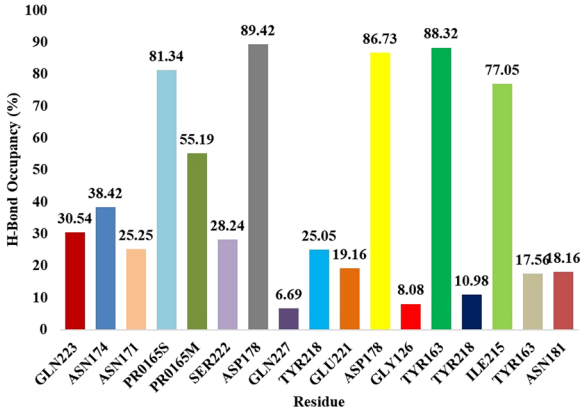

FIGURE 10 Histogram representation of %occupancies of the H-bond protein–ligand contacts of fisetinin in complex with lactate dehydrogenase A (LDHA) protein (PDB ID: 5W8L).

TABLE 5 MMGBSA ΔG binding energy calculations for 5W8L apoprotein and Fisetin-5W8L complex.

Time (ns)	5W8L apoprotein	5W8L-Fisetin complex
0	−27.487	−28.043
50	−25.127	−36.774
100	−29.094	−36.967
Average	−27.236	−33.928

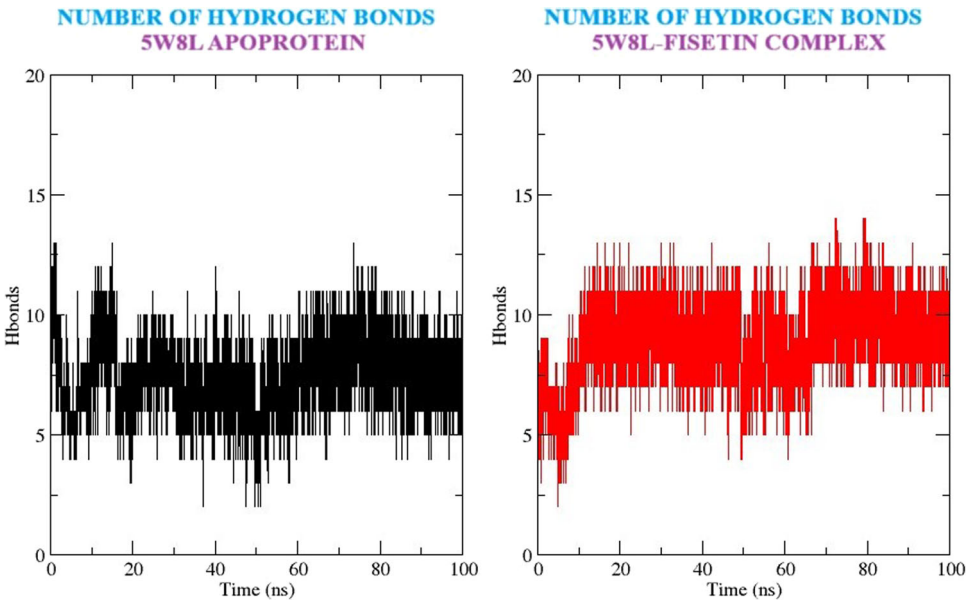

FIGURE 9 Pictorial representation of the number of h-bond contacts formed by ligands, (a) 5W8L apoprotein, and (b) fisetin in complex with lactate dehydrogenase A (LDHA) protein (PDB ID: 5W8L).

15214184, 2024, 9, Downloaded from https://onlinelibrary.wiley.com/doi/10.1002/ardp.202400455 by Kirikkale University, Wiley Online Library on [30/06/2025]. See the Terms and Conditions (https://onlinelibrary.wiley.com/terms-and-conditions) on Wiley Online Library for rules of use; OA articles are governed by the applicable Creative Commons License

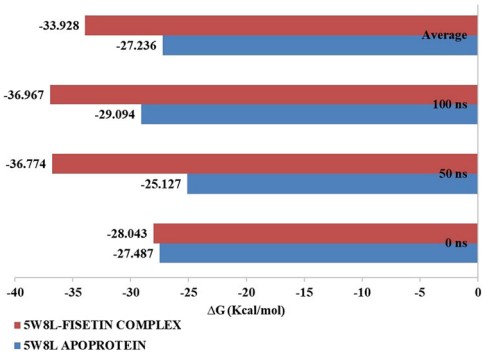

FIGURE 11 MMGBSA ΔG binding energy calculations for 5W8L apoprotein and fisetin-5W8L complex.

4.3.2 | Setting up a system for simulation

After applying the force field, the complexes were inserted into the system. They were solvated with the TIP3P water model [27] in a cubic box greater than 1 nm from the edge of the protein with periodic boundary conditions. The system was neutralized by adding Na^+ ions, and energy minimization was done for 50,000 steps using the steepest descent algorithm. It was then followed by 100 ps of NVT simulation at 300 K and 100 ps of NPT simulation to equilibrate the whole system. The Leapfrog algorithm was employed in the constant-temperature, constant-pressure (NPT) ensemble to separately couple each component like protein, ligand, water molecules, and ions.[28] The Berendsen temperature and pressure coupling constants were set to 0.1 and 2 to keep the system in a stable environment (300 K temperature and 1 bar pressure).[29] Finally, MD simulation for 100 ns was performed in isothermal and isobaric condition ensemble at 300 K. The pressure coupling with time-constant was set at one ps to maintain pressure constant at 1 bar, and the LINCS algorithm[30] was used to constrain the bond lengths. The Van der Waals and Coulomb interactions were truncated at 1.2 nm, and the PME algorithm[31] built in GROMACS was used to minimize the error from truncation.

4.3.3 | Visualization and analysis of simulation

The trajectory files are visualized through VMD (Visual Molecular Dynamics) 1.9.2.[32] Maestro 2022.4 academic version and analyzed by indigenously developed tool HeroMDAnalysis[33,34] and Xmgrace 5.1.25.[35]

4.4 | Statistical analysis

The flavonoid samples were analyzed in triplicate, and the IC_{50} and K_i values are presented as the mean ± standard deviation (SD). The statistical significance of the differences between the means was determined by analysis of variance followed by Tukey's multiple comparisons at $p < 0.05$. The statistical analyses were conducted using the R software version 4.4.0.

ACKNOWLEDGMENTS

All experimental studies were carried out at Kırıkkale University Scientific and Technological Researches Application and Research Centre Directorate (KÜBTUAM).

DATA AVAILABILITY STATEMENT

Research data are not shared.

ORCID

Ümit Yırtıcı http://orcid.org/0000-0002-0142-6105

REFERENCES

[1] R. Rani, V. Kumar, *J. Med. Chem.* **2016**, *59*, 487. https://doi.org/10.1021/acs.jmedchem.5b00168
[2] D. Sharma, M. Singh, R. Rani, *Semin. Cancer Biol.* **2022**, *87*, 184. https://doi.org/10.1016/j.semcancer.2022.11.007
[3] S. Shibata, S. Sogabe, M. Miwa, T. Fujimoto, N. Takakura, A. Naotsuka, S. Kitamura, T. Kawamoto, T. Soga, *Sci. Rep.* **2021**, *11*, 21353. https://doi.org/10.1038/s41598-021-00820-7
[4] C. Wang, Y. Li, S. Yan, H. Wang, X. Shao, M. Xiao, B. Yang, G. Qin, R. Kong, R. Chen, N. Zhang, *Nat. Commun.* **2020**, *11*, 3162. https://doi.org/10.1038/s41467-020-16966-3
[5] R. E. Mutha, A. U. Tatiya, S. J. Surana, *Fut. J. Pharmaceut. Sci.* **2021**, *7*, 25. https://doi.org/10.1186/s43094-020-00161-8
[6] H. Yao, F. Yang, Y. Li, *Front. Chem.* **2022**, *10*, 1013670. https://doi.org/10.3389/fchem.2022.1013670
[7] M. Samec, A. Liskova, L. Koklesova, S. M. Samuel, K. Zhai, C. Buhrmann, E. Varghese, M. Abotaleb, T. Qaradakhi, A. Zulli, M. Kello, J. Mojzis, P. Zubor, T. K. Kwon, M. Shakibaei, D. Büsselberg, G. R. Sarria, O. Golubnitschaja, P. Kubatka, *EPMA J.* **2020**, *11*, 377. https://doi.org/10.1007/s13167-020-00217-y
[8] J. Hughes, S. Rees, S. Kalindjian, K. Philpott, *Br. J. Pharmacol.* **2011**, *162*, 1239. https://doi.org/10.1111/j.1476-5381.2010.01127.x
[9] J. H. Han, E.-J. Lee, W. Park, K.-T. Ha, H.-S. Chung, *Front. Pharmacol.* **2023**, *14*. https://doi.org/10.3389/fphar.2023.1275000
[10] M. Manerba, M. Vettraino, L. Fiume, G. Di Stefano, A. Sartini, E. Giacomini, R. Buonfiglio, M. Roberti, M. Recanatini, *Chem. Med. Chem* **2012**, *7*, 311. https://doi.org/10.1002/cmdc.201100471
[11] A. Bader, T. Tuccinardi, C. Granchi, A. Martinelli, M. Macchia, F. Minutolo, N. De Tommasi, A. Braca, *Phytochemistry* **2015**, *116*, 262. https://doi.org/10.1016/j.phytochem.2015.03.007
[12] M. Mazlaghaninia, M. S. Atri, B. Seyedalipour, *Hormozgan Med. J.* **2019**, *23*, e88269. https://doi.org/10.5812/hmj.88269
[13] G. S. Prasath, S. P. Subramanian, *Eur. J. Pharmacol.* **2011**, *668*, 492. https://doi.org/10.1016/j.ejphar.2011.07.021
[14] K. Sundarraj, A. Raghunath, E. Perumal, *Biomed. Pharmacother.* **2018**, *97*, 928. https://doi.org/10.1016/J.BIOPHA.2017.10.164
[15] R. I. Troup, C. Fallan, M. G. J. Baud, *Explor. Target. Anti-tumor Ther.* **2020**, *1*, 273. https://doi.org/10.37349/etat.2020.00018
[16] Ş. Adem, Ü. Yırtıcı, M. Aydın, R. Rawat, V. Eyüpoğlu, *Arch. Pharm. (Weinheim)* **2024**, *357*, 2300326. https://doi.org/10.1002/ardp.202300326
[17] A. Karmakar, K. Karthick, S. S. Sankar, S. Kumaravel, R. Madhu, S. Kundu, *J. Mater. Chem. A* **2021**, *9*, 1314. https://doi.org/10.1039/D0TA09788H
[18] F. Shapiro, N. Silanikove, *Food. Chem.* **2010**, *119*, 829. https://doi.org/10.1016/j.foodchem.2009.07.029
[19] C. Yung-Chi, W. H. Prusoff, *Biochem. Pharmacol.* **1973**, *22*, 3099. https://doi.org/10.1016/0006-2952(73)90196-2

15214184, 2024, 9, Downloaded from https://onlinelibrary.wiley.com/doi/10.1002/ardp.202400455 by Kirikkale University, Wiley Online Library on [30/06/2025]. See the Terms and Conditions (https://onlinelibrary.wiley.com/terms-and-conditions) on Wiley Online Library for rules of use; OA articles are governed by the applicable Creative Commons License

[20] R. Thomsen, M. H. Christensen, *J. Med. Chem.* **2006**, *49*, 3315. https://doi.org/10.1021/jm051197e

[21] G. Rai, K. R. Brimacombe, B. T. Mott, D. J. Urban, X. Hu, S.-M. Yang, T. D. Lee, D. M. Cheff, J. Kouznetsova, G. A. Benavides, K. Pohida, E. J. Kuenstner, D. K. Luci, C. M. Lukacs, D. R. Davies, D. M. Dranow, H. Zhu, G. Sulikowski, W. J. Moore, G. M. Stott, A. J. Flint, M. D. Hall, V. M. Darley-Usmar, L. M. Neckers, C. V. Dang, A. G. Waterson, A. Simeonov, A. Jadhav, D. J. Maloney, *J. Med. Chem.* **2017**, *60*, 9184. https://doi.org/10.1021/acs.jmedchem.7b00941

[22] H. Bekker, H. J. C. Berendsen, E. J. Dijkstra, S. Achterop, R. van Drunen, D. van der Spoel, A. Sijbers, H. Keegstra, *Phys. Comp.* **1993**, *92*, 252.

[23] A. Ganesan, M. L. Coote, K. Barakat, *Drug Discovery Today* **2017**, *22*, 249. https://doi.org/10.1016/j.drudis.2016.11.001

[24] S. A. Arvindekar, S. Mohole, A. Patil, P. Mane, A. Arvindekar, S. N. Mali, B. Thorat, R. Rawat, S. Sharma, *J. Biomol. Struct. Dyn.* **2023**, *41*, 14757. https://doi.org/10.1080/07391102.2023.2190803

[25] N. Schmid, A. P. Eichenberger, A. Choutko, S. Riniker, M. Winger, A. E. Mark, W. F. van Gunsteren, *Eur. Biophys. J.* **2011**, *40*, 843. https://doi.org/10.1007/s00249-011-0700-9

[26] D. M. F. van Aalten, R. Bywater, J. B. C. Findlay, M. Hendlich, R. W. W. Hooft, G. Vriend, *J. Comput. Aided. Mol. Des.* **1996**, *10*, 255. https://doi.org/10.1007/BF00355047

[27] P. Mark, L. Nilsson, *J. Phys. Chem. A* **2001**, *105*, 9954. https://doi.org/10.1021/jp003020w

[28] W. F. Van Gunsteren, H. J. C. Berendsen, *Mol. Simul.* **1988**, *1*, 173. https://doi.org/10.1080/08927028808080941

[29] H. J. C. Berendsen, D. van der Spoel, R. van Drunen, *Comput. Phys. Commun.* **1995**, *91*, 43. https://doi.org/10.1016/0010-4655(95)00042-E

[30] B. Hess, H. Bekker, H. J. C. Berendsen, J. G. E. M. Fraaije, *J. Comput. Chem.* **1997**, *18*, 1463. https://doi.org/10.1002/(SICI)1096-987X(199709)18:12<1463::AID-JCC4>3.0.CO;2-H

[31] M. Di Pierro, R. Elber, B. Leimkuhler, *J. Chem. Theory. Comput.* **2015**, *11*, 5624. https://doi.org/10.1021/acs.jctc.5b00648

[32] W. Humphrey, A. Dalke, K. Schulten, *J. Mol. Graph.* **1996**, *14*, 33. https://doi.org/10.1016/0263-7855(96)00018-5

[33] R. Rawat, K. Kant, A. Kumar, K. Bhati, S. M. Verma, *Future Med. Chem.* **2021**, *13*, 447. https://doi.org/10.4155/fmc-2020-0191

[34] B. Sahu, R. Bhatia, D. Kaur, D. Choudhary, R. Rawat, S. Sharma, B. Kumar, *Bioorg. Chem.* **2023**, *136*, 106544. https://doi.org/10.1016/j.bioorg.2023.106544

[35] A. Vaught, *Graphing with Gnuplot and Xmgr*, **1996**. http://www.linuxjournal.com/article/1218

How to cite this article: Ü. Yırtıcı, *Arch. Pharm.* **2024**;*357*:e2400455. https://doi.org/10.1002/ardp.202400455

15214184, 2024, 9, Downloaded from https://onlinelibrary.wiley.com/doi/10.1002/ardp.202400455 by Kirikkale University, Wiley Online Library on [30/06/2025]. See the Terms and Conditions (https://onlinelibrary.wiley.com/terms-and-conditions) on Wiley Online Library for rules of use; OA articles are governed by the applicable Creative Commons License